*Int. J. Heat Mass Transfer.* Vol. 29, No. 11, pp. 1747–1758, 1986
Printed in Great Britain

0017–9310/86 $3.00 + 0.00
Pergamon Journals Ltd.

# Conjugate film condensation and natural convection along the interface between a porous and an open space

D. POULIKAKOS and P. SURA

Department of Mechanical Engineering, University of Illinois at Chicago,
P.O. Box 4348, Chicago, IL 60680, U.S.A.

(*Received* 17 *September* 1985 *and in final form* 25 *March* 1986)

**Abstract**—This paper reports a theoretical investigation focusing on the interaction between film condensation and natural convection along a vertical wall separating a fluid reservoir from a fluid-saturated porous reservoir. The two reservoirs are maintained at different temperatures. The study consists of two parts: in the first part the condensation phenomenon takes place in the fluid reservoir and the natural convection phenomenon in the porous layer. In the second part, the opposite situation is considered. The main heat transfer and flow characteristics in the two counterflowing layers, namely, the condensation film and the natural convection boundary layer are documented for a wide range of the problem parameters. These parameters appear after boundary layer scaling of the governing equations. Important engineering results regarding the overall heat flux from the condensation side to the natural convection side are summarized in the course of the study. Finally, the effect of the thermal resistance of the wall constituting the interface separating the two reservoirs, on the overall heat flux from the condensation side to the natural convection side is determined.

## 1. INTRODUCTION

COUPLING between two distinct heat transfer modes through a solid boundary finds a host of applications in heat transfer engineering. The present paper focuses on the investigation of such coupling between film condensation on the one side of a vertical boundary and natural convection on the other side. The boundary of interest constitutes the interface between a fluid space on the one hand, and a fluid-saturated porous space on the other hand. This configuration occurs in thermal insulations, heat exchangers, buildings, cryogenic equipment and grain storage. In addition, the geometry under investigation is of geophysical interest.

The importance of the problem of thermal interaction in natural convection flows has been recognized by several previous investigators [1–5]. Such flows are solely driven by temperature gradients, hence, they appear to be sensitive to temperature changes imposed in the domain in which the flows take place. Lock and Ko [1] have shown, via finite-difference calculations, that two counterflowing natural convection boundary layers coupled through a vertical wall constitute a heat transfer system noticeably different from that featuring a prescribed temperature or heat flux on the wall [2]. More recently, Bejan and Anderson report interesting results pertinent to natural convection interaction in three distinct geometries: at the interface between a vertical porous layer and an open space [3]; at the interface between two porous layers [4]; and at the interface between two fluid layers [5]. The problems in [3–5] are solved theoretically based on the Oseen-linearization method used first by Gill [6] who investigated natural convection in a vertical slot. The effect of the thermal resistance of the wall separating the two reservoirs was accounted for in refs. [4, 5] while it was omitted for simplicity in refs. [1, 3]. The approximate theoretical findings in ref. [5] agreed well with the more exact numerical calculations reported in ref. [1] in the limit of low wall thermal resistance. Sparrow and Prakash [7] investigated the effect of interaction between natural convection in a rectangular enclosure and an external natural convection boundary layer developing along one of the enclosure walls. These authors proved that such interaction forces this wall to depart from the uniform temperature or uniform flux condition used in numerous basic research studies. In addition, the heat transfer and flow characteristics of the system in ref. [7] were noticeably different from those reported for the classical enclosure model [8, 9].

In this study we focus on conjugate natural convection and film condensation along the impermeable interface of a porous layer and a fluid space. The study consists of two distinct parts: in the first part the condensation takes place in the fluid space and the fluid-saturated porous layer models an insulation support separating the condensation space form its cold surroundings. In the second part our attention is shifted to the configuration where the condensation phenomenon takes place in the porous space. Here, the open space plays the role of the cold reservoir. Both parts of the study are analyzed based on the Oseen-linearization method for the natural convection side [6] and thin film analysis for the condensation side [2, 10]. The solution is completed by matching the findings from each side on the wall. Unlike the classical problem of natural convection and condensation in classical fluids [2] and in porous media [11–13] here, the wall temperature and the wall

## NOMENCLATURE

| | |
|---|---|
| $A$ | dimensionless group, equation (18) |
| $B$ | dimensionless group, equation (15) |
| $c_p$ | fluid specific heat at constant pressure |
| $D$ | dimensionless group, equation (23) |
| $Da$ | Darcy number, equation (6) |
| $E$ | dimensionless group, equation (5) |
| $g$ | gravitational acceleration |
| $G$ | dimensionless group, equation (27) |
| $H$ | wall height |
| $h_{fg}$ | latent heat of condensation |
| $K$ | permeability |
| $k$ | fluid thermal conductivity |
| $k_p$ | effective thermal conductivity of porous medium |
| $m$ | Oseen's function |
| $N$ | dimensionless group, equation (22) |
| $Nu$ | Nusselt number |
| $Pr$ | Prandtl number, $\nu/\alpha$ |
| $Ra$ | Rayleigh number based on the wall height, $g\beta H^3(T_s-T_c)/\nu\alpha$ |
| $Ra_f$ | film Rayleigh number based on the wall height, equation (14) |
| $Ra_p$ | Darcy-modified Rayleigh number based on the wall height, equation (7) |
| $t$ | wall thickness, Fig. 1a |
| $T$ | temperature |
| $u$ | horizontal velocity component |
| $v$ | vertical velocity component |
| $x$ | horizontal Cartesian coordinate |
| $y$ | vertical Cartesian coordinate. |

Greek symbols

| | |
|---|---|
| $\alpha$ | fluid thermal diffusivity, $k/\rho c_p$ |
| $\alpha_p$ | effective thermal diffusivity of porous medium, $k_p/\rho c_p$ |
| $\beta$ | coefficient of thermal expansion |
| $\gamma$ | Oseen's function |
| $\delta$ | boundary-layer thickness scale, Fig. 1 |
| $\zeta$ | condensation film thickness |
| $\mu$ | viscosity |
| $\nu$ | kinematic viscosity, $\mu/\rho$ |
| $\rho$ | fluid density |
| $\omega$ | wall thermal resistance parameter. |

Subscripts

| | |
|---|---|
| c | cold |
| f | condensation film |
| l | liquid phase for condensation in open reservoir |
| p | porous |
| pl | liquid phase for condensation in porous reservoir |
| pv | vapor phase for condensation in porous reservoir |
| s | saturation |
| v | vapor phase for condensation in open reservoir |
| w | wall |
| wL | left side of wall |
| wR | right side of wall |
| * | dimensionless quantity for open reservoir condensation |
| I | pertaining to Part I of the paper |
| II | pertaining to Part II of the paper. |

Symbols

| | |
|---|---|
| ^ | dimensional quantity |
| ~ | dimensionless quantity for natural convection in open reservoir |
| - | dimensionless quantity for condensation in porous reservoir. |

heat flux are unknowns to be determined by the problem solution. The only study featuring this characteristic and relevant to conjugate condensation and convection we are familiar with, is ref. [14]. In this reference, Sparrow and Faghri investigate the effect of external condensation on the heat losses from an internally cooled vertical tube.

Results documenting the effect of finite thermal resistance at the interface of the two media on the heat transfer from the hot to the cold space are also reported in the course of the present study.

## 2. MATHEMATICAL MODEL

The configurations of interest are shown schematically in Fig. 1. Figure 1a depicts the arrangement pertinent to the first part of the study: a solid wall separating a porous from a fluid space. The fluid space contains vapor at saturation temperature, $T_s$, and is the warmer of the two spaces. The porous space is fluid saturated and is maintained at $T_c$ where $T_c < T_s$. The cooling effect of the porous layer is felt by the vapor in the warm reservoir through the diathermal wall. It is assumed that this cooling effect results in film condensation in the open space. At the same time, the heating effect of the open space initiates an upward moving, buoyancy driven, fluid jet in the wall vicinity within the porous layer. The two fluid jets, i.e. the condensation film and the natural convection boundary layer, move in opposite directions while exchanging heat through the solid interface in a manner similar to the operation of a counterflow heat exchanger.

The description of the configuration shown in Fig. 1b, which illustrates the problem tackled in the second

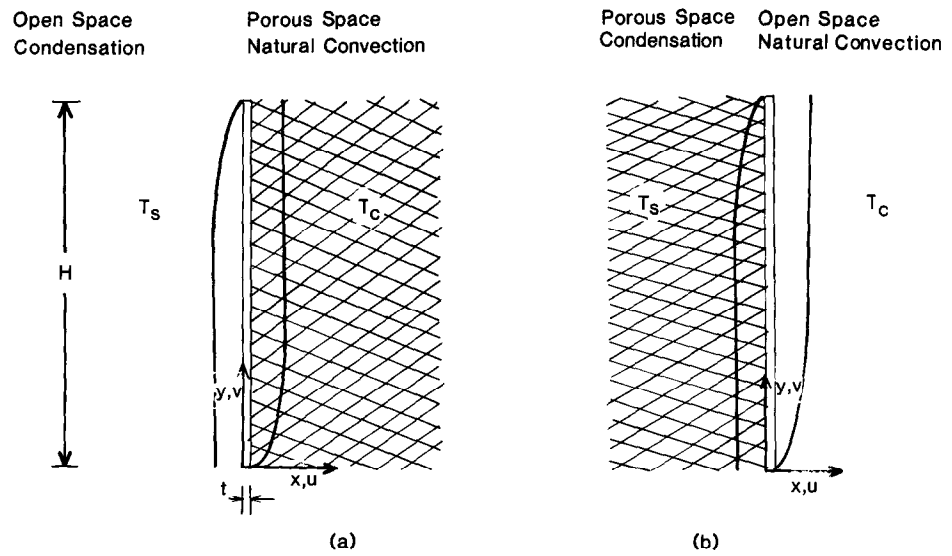


FIG. 1. Schematic of the problem of interest. (a) Natural convection in the porous side of the interface and condensation in the open side. (b) Natural convection in the open side of the interface and condensation in the porous side.

part of the study, is analogous to the above with the exception that in this case the condensation phenomenon takes place in the porous reservoir which is kept at $T_s$, and the natural convection phenomenon in the open reservoir which is kept at $T_c$. Next, both parts of the problem of interest are formulated mathematically by considering the natural convection side and the condensation side separately.

*Part I. Porous space natural convection and open space condensation*

*Ia. Porous space.* The Brinkman modification of the Darcy flow model [11, 12] is used to describe the natural convection phenomenon in the porous reservoir. The Brinkman model, unlike the Darcy model, satisfies the no-slip condition on a solid boundary and has been proven appropriate for flows near solid boundaries [15–17]. The dimensionless *boundary-layer* equations describing the conservation of mass, momentum and energy at each point in the porous medium are:

$$\frac{\partial u}{\partial x}+\frac{\partial v}{\partial y}=0 \tag{1}$$

$$\frac{\partial v}{\partial x}=E\frac{\partial^3 v}{\partial x^3}+\frac{\partial T}{\partial x} \tag{2}$$

$$u\frac{\partial T}{\partial x}+v\frac{\partial T}{\partial y}=\frac{\partial^2 T}{\partial x^2}. \tag{3}$$

The non-dimensionalization in (1)–(3) was based on the following definitions:

$$x=\frac{\hat{x}}{HRa_p^{-1/2}},\quad y=\frac{\hat{y}}{H},\quad u=\frac{\hat{u}}{(\alpha_p/HRa_p^{-1/2})},$$
$$v=\frac{\hat{v}}{[\alpha_p H/(HRa_p^{-1/2})^2]},\quad T=\frac{\hat{T}+\frac{1}{2}(T_s-T_c)}{T_s-T_c}. \tag{4}$$

The dimensionless quantities in equation (4) were defined based on boundary-layer scaling for natural convection problems (see for example refs. [18–20]). The details of such scaling are omitted here for brevity, however, attention should be drawn to the fact that the scale of the boundary-layer thickness ($\delta \sim HRa_p^{-1/2}$) was used to non-dimensionalize the horizontal coordinate $\hat{x}$. Parameter $E$ in equation (2) is given by

$$E=Da\,Ra_p \tag{5}$$

where $Da$ and $Ra_p$ are the Darcy number and the Darcy-modified Rayleigh number, respectively

$$Da=\frac{K}{H^2}, \tag{6}$$

$$Ra_p=\frac{Kg\beta(T_s-T_c)H}{\nu\alpha_p}. \tag{7}$$

Equation (2) was derived by eliminating the pressure gradient between the $x$ and $y$ momentum equations and by taking into account the Boussinesq approximation for natural convection, whereby the density was assumed to be constant everywhere except in the buoyancy term of the momentum equation where its dependence on temperature was described by

$$\rho=\rho_0[1-\beta(\hat{T}-T_0)]. \tag{8}$$

In the above equation subscript zero stands for a reference state. All the symbols in equations (1)–(8) not defined in the text are defined in the Nomenclature. The boundary conditions for the porous medium side in Part I of this study are

$$\begin{aligned} &u=v=0, && T=T_w(y) && \text{at } x=0\\ &v=0, && T=-1/2 && \text{at } x\to\infty. \end{aligned} \tag{9}$$

One more condition at the interface ($x=0$), namely,

the heat flux continuity, will be discussed after the mathematical formulation for the condensation side has been completed.

*Ib. Open space.* The classical solution for film condensation along a vertical wall [2, 10] yields

$$v_* = \left(\zeta x_* + \frac{x_*^2}{2}\right) \tag{10}$$

$$T = (-\tfrac{1}{2}+T_w)\frac{x_*}{\zeta} + T_w \tag{11}$$

$$\zeta^3 \frac{d\zeta}{dy} = \frac{\frac{1}{2}-T_w}{1+B(\frac{1}{2}-T_w)}. \tag{12}$$

The dimensionless parameters for the condensation side are defined as follows

$$(x_*, \zeta) = (\hat{x}, \hat{\zeta})/HRa_f^{-1/4},$$

$$v_* = \hat{v}\Big/\left[\frac{g(\rho_l-\rho_v)}{\mu_l}(HRa_f^{-1/4})^2\right]. \tag{13}$$

In the above definitions $Ra_f$ is the film Rayleigh number,

$$Ra_f = \frac{H^3 g(\rho_l-\rho_v)h_{fg}}{k_l\nu_l(T_s-T_c)} \tag{14}$$

and $B$ is a dimensionless parameter measuring the degree of subcooling in the film

$$B = \tfrac{3}{8}c_p\frac{T_s-T_c}{h_{fg}}. \tag{15}$$

Subscripts l and v stand for liquid and vapor phases, respectively, and $h_{fg}$ is the latent heat of condensation. It is worth noting that solution (10)–(12) satisfies the following boundary conditions

$$\begin{aligned} &v_* = 0, \quad T = T_w(y) \quad \text{at } x_* = 0 \\ &\frac{\partial v_*}{\partial x_*} = 0, \quad T = \tfrac{1}{2} \quad \text{at } x_* = -\zeta. \end{aligned} \tag{16}$$

Implicit in equations (9) and (16) is the assumption that the solid wall at the interface of the two reservoirs is thin or of large thermal conductivity. Hence, the temperature drop across the wall is neglected compared with the reservoir-to-reservoir temperature difference. The effect of finite thermal resistance at the interface will be investigated in a later section of the study. Based on the above assumption the last matching condition at the interface, namely, the heat flux continuity statement reads

$$A\left(\frac{\partial T}{\partial x_*}\right)_{x_*=0^-} = \left(\frac{\partial T}{\partial x}\right)_{x=0^+} \tag{17}$$

where

$$A = \frac{k_l}{k_p}\frac{Ra_p^{-1/2}}{Ra_f^{-1/4}}. \tag{18}$$

At this point, the first part of the study is thoroughly formulated. Before proceeding to the solution of Part I, the second part of the study will be formulated next.

*Part II. Open space natural convection, porous space condensation*

The pertinent dimensionless boundary-layer equations and boundary conditions for the natural convection side of the system shown in Fig. 1b have been reported in refs. [3, 5, 21]. Hence, they are omitted here for brevity. All the details pertinent to the present problem were included in ref. [21]. It is worth stressing that much like in refs. [3, 5] the momentum equations in the present study are accurate in the limit where $Pr > O(1)$ (the inertia terms have been neglected). It has been shown however [3, 5], that neglecting the inertia terms in the momentum equation yields acceptable results (accurate within 10%) even for $Pr = O(1)$. In this section, only the mathematical model for the condensation side will be described.

The phenomenon of two-phase flow in porous medium is a complex one because of the fact that the pore spaces are filled partly with vapor and partly with liquid. To account for this fact the concept of relative permeability is introduced in the mathematical modeling of two-phase flow in porous medium, in conjunction with existing models for single-phase convection such as the Darcy model and the Brinkman-modified Darcy model. However, as discussed by Cheng [22], due to the mathematical complexity of the governing equations for two-phase flows in porous media involving the concept of relative permeability, analytical solutions can be obtained only after the following simplifying assumption: the condensate and the vapor are separated by a distinct boundary with no two-phase region in between. Hence, the difficulty associated with the relative permeability is removed and the single-phase equations can be applied separately to the vapor and the condensate. This assumption was also used by Parmentier [23] to study the problem of film boiling in porous medium.

The solution for thin film condensation in the porous side of the interface of the system shown in Fig. 1b was obtained by using the Brinkman flow model for the condensate zone and the above simplifying assumptions. The procedure is identical to that used for classical fluids [2, 10] therefore, no intermediate steps are shown here. However, all the intermediate steps are reported in ref. [21]. The final results read

$$\bar{v} = \left[\frac{\cosh K^{-1/2}(\bar{\zeta}+\bar{x})}{\cosh K^{-1/2}\bar{\zeta}} - 1\right] \tag{19}$$

$$T = -(\tfrac{1}{2}-T_w)\frac{\bar{x}}{\bar{\zeta}} + T_w \tag{20}$$

$$\frac{dy}{d\bar{\zeta}} = -\bar{\zeta}(\operatorname{sech}^2(N\bar{\zeta})-1)\left\{\frac{1}{\frac{1}{2}-T_w} + D\left(1 - \frac{(2-N^2\bar{\zeta}^2)\cosh N\bar{\zeta}-2}{2N\bar{\zeta}\cosh N\zeta(\tanh N\bar{\zeta}-N\bar{\zeta})}\right)\right\} \tag{21}$$

where

$$N = Da^{-1/2} Ra_{pf}^{-1/2}, \tag{22}$$

$$D = \frac{c_p(T_s - T_c)}{h_{fg}}. \tag{23}$$

The Darcy-modified film Rayleigh number for porous medium condensation in equation (22) is defined as

$$Ra_{pf} = \frac{HK(\rho_l - \rho_v)gh_{fg}}{k_p \nu_p (T_s - T_c)}. \tag{24}$$

The non-dimensionalization of equations (19)–(21) was carried out based on the following definitions

$$(\bar{x}, \bar{\zeta}) = (\hat{x}, \hat{\zeta})/HRa_{pf}^{-1/2},$$

$$\bar{v} = \hat{v} \Big/ \frac{(\rho_l - \rho_v)gK}{\mu}. \tag{25}$$

The dimensionless temperature was obtained via equation (4). It is worth noting that solutions (19)–(21) satisfy a set of boundary conditions analogous to equation (16) of Part I of this paper. The last condition to be satisfied is that of continuous wall heat flux

$$G\left(\frac{\partial T}{\partial \bar{x}}\right)_{\bar{x}=0^-} = \left(\frac{\partial T}{\partial \bar{x}}\right)_{\bar{x}=0^+} \tag{26}$$

where

$$G = \frac{k_{pl}}{k} \frac{Ra^{-1/4}}{Ra_{pf}^{-1/2}}, \tag{27}$$

$$\bar{x} = x/(HRa^{-1/4}). \tag{28}$$

In this part of the study as well, the thermal resistance of the wall at the interface has been neglected for simplicity. The effect of finite wall thermal resistance will be investigated in a later section.

## 3. THEORETICAL SOLUTION

The same solution methodology was employed to attack both parts of the study. Therefore, a detailed description of the solution procedure for the first part of the study only will be outlined and key results of the solution procedure for the second part will be reported. Since the expressions for the temperature and the velocity distributions as well as the condensation film thickness for the left side of the configuration shown in Fig. 1a have been reported in the previous section, equations (10)–(12), here, we will focus on the Oseen-linearized solution for the porous space. According to the Oseen linearization method [3–6, 24] the horizontal velocity component $u$ and the temperature gradient in the vertical $\partial T/\partial y$ are assumed to be unknown functions of altitude, $u_A(y)$ and $T'_A(y)$ in the energy equation (3). Based on this assumption and eliminating $\partial T/\partial x$ and $\partial^2 T/\partial x^2$ from equation (3) by employing equation (2) we obtain

$$\frac{\partial^4 v}{\partial x^4} - u_A \frac{\partial^3 v}{\partial x^3} - \frac{1}{E}\frac{\partial^2 v}{\partial x^2} + \frac{u_A}{E}\frac{\partial v}{\partial x} + \frac{T'_A}{E} v = 0. \tag{29}$$

The solution of equation (36) has the form

$$v = \sum_{n=1}^{4} A_n(y) e^{-\lambda_n(y)x} \tag{30}$$

where $\lambda_n$ ($n = 1, \ldots, 4$) are the four roots of the characteristic equation

$$\lambda^4 + u_A \lambda^3 - \frac{1}{E}\lambda^2 - \frac{u_A}{E}\lambda + \frac{T'_A}{E} = 0. \tag{31}$$

These four roots are, in general, complex. In fact, they constitute two pairs of complex conjugate numbers. As has been discussed in detail in previous studies [3–6, 24] only the roots with *positive* real parts satisfy the condition of vanishing $v$ at infinity.

Hence

$$v = A_1(y) e^{-\lambda_1 x} + A_2(y) e^{-\lambda_2 x}. \tag{32}$$

In addition, the vertical velocity component should vanish at the wall. Taking this condition into account and substituting the resulting expression for $v$ into the momentum equation (2) we can solve for the temperature distribution. The remaining constants of integration are obtained by applying the boundary conditions for the temperature on the wall and at infinity. The final expressions for the temperature and the velocity fields read

$$v = \frac{T_w + \frac{1}{2}}{2m\gamma E} e^{-mx} \sin \gamma x \tag{33}$$

$$T = \frac{T_w + \frac{1}{2}}{2m\gamma E} e^{-mx} [\sin \gamma x - E\{(m^2 - \gamma^2)\sin \gamma x - 2m\gamma \cos \gamma x\}] - \tfrac{1}{2} \tag{34}$$

where $m$ and $\gamma$ are unknown functions of $y$ constituting the real and imaginary parts of $\lambda_1$, $\lambda_2$ respectively ($\lambda_{1,2} = m \pm i\gamma$). Two additional conditions for $m$ and $\gamma$ are obtained by satisfying the energy equation on the wall ($x = 0$) and after it is integrated over the entire boundary-layer thickness. These conditions are

$$\gamma^2 = \left(\frac{2m^2E - 1}{2E}\right) \tag{35}$$

$$\frac{d}{dy}\left\{\left(\frac{T_w + \frac{1}{2}}{2m\gamma E}\right)^2 \left[[1 - E(m^2 - \gamma^2)] \times \left(\frac{1}{4m} - \frac{m}{4(m^2 + \gamma^2)}\right) + \frac{Em\gamma^2}{2(m^2 + \gamma^2)}\right]\right\} = -\frac{T_w + \frac{1}{2}}{2mE}(\gamma^2 E - 3m^2 E + 1). \tag{36}$$

Next, combining the flux continuity condition (17), with the temperature relations (11), (34) yields

$$A\frac{T_w - \frac{1}{2}}{T_w + \frac{1}{2}} = \frac{\zeta}{2mE}(\gamma^2 E - 3m^2 E + 1). \tag{37}$$

At this point we are left with four equations (12), (35), (36), (37) containing four unknowns ($\zeta$, $T_w$, $m$, $\gamma$).

Noting that we can use equation (35) to eliminate $\gamma$ from equations (36) and (37) yields three equations containing three unknowns ($\zeta$, $T_w$, $m$). The number of equations is reduced further by solving equation (37) for $m$ explicitly and substituting the result into equation (36). The final set of two equations with two unknowns $T_w$ and $\zeta$ is reported in the Appendix [equations (A1)–(A3)]. This set of equations is solved numerically to yield the wall temperature distribution and the condensation film thickness.

The two counterflowing boundary layers exchange heat much like in a very long counterflow heat exchanger. Hence, the wall temperature $T_w(y)$ assumes values between the two reservoir temperatures, $-\frac{1}{2}$ and $\frac{1}{2}$. It was found that when equations (A1) and (A2) were cast in a different form, i.e. by using the vertical coordinate $y$ as the independent variable (which appeared to be the natural choice), the RHS of the equation corresponding to (A2) blew up at $y = 0$ ($T_w = -\frac{1}{2}$). This difficulty was overcome by using the wall temperature as the independent variable and the condensation film thickness, $\zeta$, and the altitude, $y$, as the dependent variables. The simultaneous numerical integration of equations (A1) and (A2) was performed by using the Runge–Kutta method [25, 26]. To start the integration, initial values (at $y = 0$) for both $y$ and $\zeta$ were required. The initial value of $y$ is known: $y = 0$. However, the value of the condensation thickness $\zeta$ at $y = 0$ is not known. Consequently, an iterative process was followed: the initial value of $\zeta$ was guessed and the integration in $T_w$ followed next by starting at $T_w = -\frac{1}{2}$ and by advancing in small steps in $T_w$ until the other extreme of the $T_w$-range ($T_w = \frac{1}{2}$) was reached. The value of $y$ at which $T_w = \frac{1}{2}$ was then checked. The above procedure was repeated by adjusting the initial value of $\zeta$ so that eventually $T_w = \frac{1}{2}$ corresponded to $y = 1$. The 'step' in $T_w$ was small enough so that reducing this step further had no effect on the results. It was found that using 5000 equally sized steps to bridge the gap between $-\frac{1}{2} \leqslant T_w \leqslant \frac{1}{2}$ yielded results accurate to the fourth decimal point.

The solution of the problem in the second part of this study was carried out by the above procedure as well [21]. After manipulations similar to Part I of this study two equations are obtained, (A4) and (A5), which are solved numerically to yield $y$ and $\bar{\zeta}$.

## 4. RESULTS AND DISCUSSION

The main results of the first part of the study are shown in Figs. 2–6. Figures 2 and 3 show representative velocity and temperature distributions in the counterflowing layers on both sides of the wall at midheight ($y = \frac{1}{2}$). Parameter $A$ has a profound effect on both temperature and velocity fields. As $A$ becomes larger than unity the temperature drop across the natural convection jet in the porous layer exceeds the temperature drop across the condensation film (Fig. 3). Based on this behavior the vertical velocity increases in the porous side and decreases in the open side (Fig. 2). Qualitatively similar, but weaker, effects on the velocity and temperature distributions are observed when varying $B$ and $E$. With reference to parameter $E$ in particular, it is found that decreasing $E$ shifts the velocity closer to the interface (Fig. 2). This result makes sense physically since small values of $E$ correspond to small values of the Darcy number

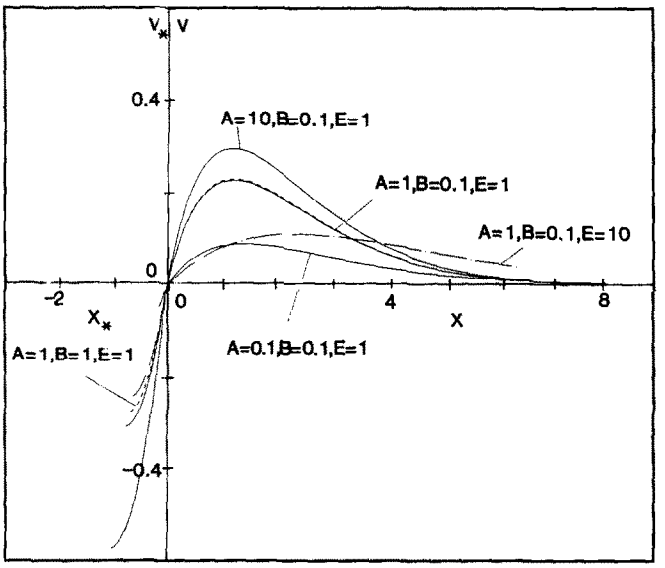


FIG. 2. Velocity profiles in the natural convection boundary layer (right) and condensation film (left) at mid-height for representative values of $A$, $B$ and $E$. The solid lines are for $E = 1$, $B = 0.1$ and depict the effect of $A$. The dashed lines correspond to $E = 1$, $A = 1$ and the dash-dot lines correspond to $B = 0.1$, $A = 1$.

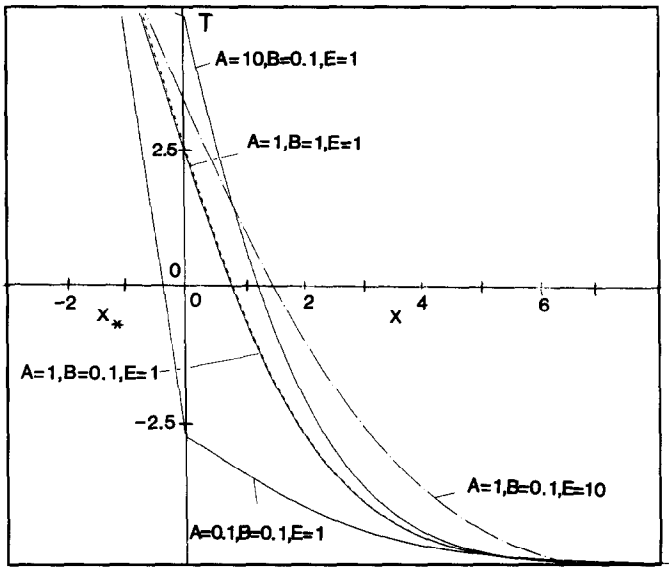


FIG. 3. Temperature profiles in the natural convection boundary layer (right) and condensation film (left) at mid-height for representative values of $A$, $B$ and $E$. The notation for the lines is identical to that used in Fig. 2.

if $Ra_p$ is held fixed. As $Da$ decreases we approach the limit where the Darcy flow model holds [11, 12, 15–17, 24]. In this limit the no-slip condition at the interface is not satisfied and the velocity maximum in the porous side occurs on the interface.

Figures 4 and 5 show examples of the wall temperature distribution and the wall heat flux. The wall temperature distribution increases with height in an approximately linear manner. Near the two ends of the wall where the boundary-layer approximations incorporated in the present study break down, the wall temperature departs from its linear distribution

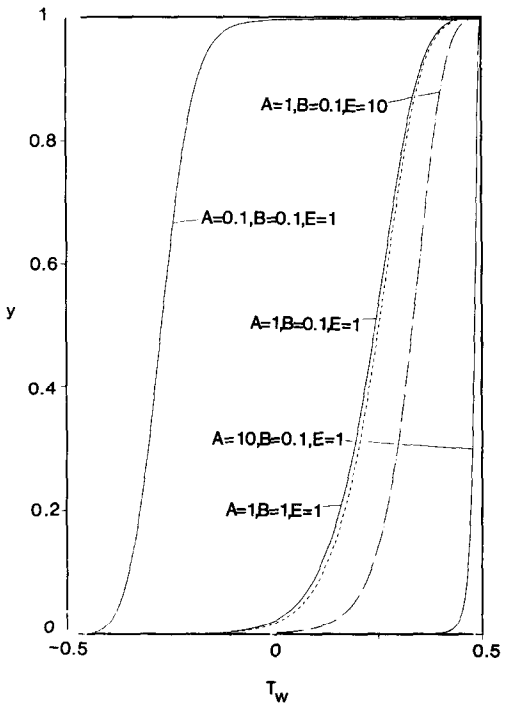


FIG. 4. The wall temperature distribution for representative values of $A$, $B$ and $E$. The notation for the lines is identical to that used in Fig. 2.

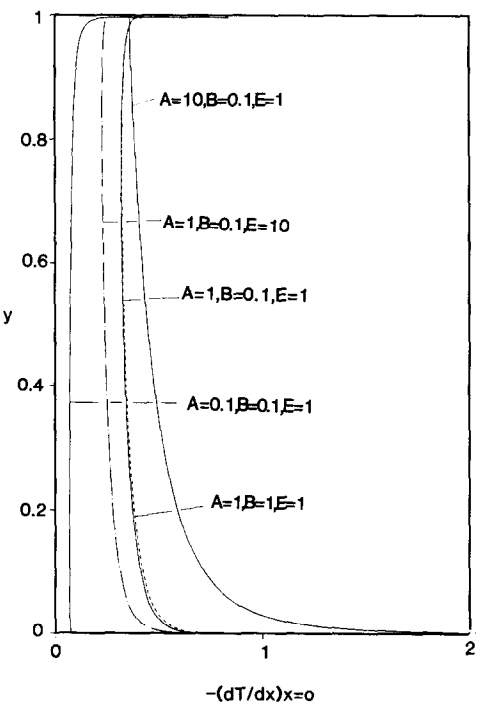


FIG. 5. The wall heat flux for representative values of $A$, $B$ and $E$. The notation for the lines is identical to that used in Fig. 2.

and assumes the values of the reservoir temperatures (Fig. 4). Increasing $A$ yields a more uniform wall temperature distribution. The trend shown in Fig. 4 implies that as $A$ becomes increasingly large the wall assumes the saturation temperature of the condensation side. This result is also supported by the temperature profiles shown in Fig. 3. Examining the definition of parameter $A$, equation (18), indicates that in the limit of large $A$ the condensation phenomenon dominates over the natural convection phenomenon, hence, the above result makes sense physically. Increasing $B$ and $E$ also forces the wall to take on increasingly higher temperatures. With reference to the heat flux distribution at the interface, Fig. 5, small values of $A$ yield a practically independent-of-altitude heat flux. Increasing $A$ and $B$ enhances the local heat flux. Near the two ends of the interface the heat flux blows up. The effect of parameter $E$ on the $x$-temperature gradient at the wall is opposite from the effect of $A$ and $B$, i.e. increasing $E$ decreases the $x$-temperature gradient. More comments on the effect of $E$ on the heat transfer through the interface will be discussed in connection with Fig. 6.

In Fig. 6 attention is shifted to obtaining heat transfer results of engineering significance. To this end, the Nusselt number is defined as follows

$$Nu_1 = \frac{Q_1}{k_p(T_s - T_c)} \tag{38}$$

where $Q_1$ is the total heat flux through the wall obtained by integrating numerically the local heat flux over the entire height of the wall. As commented in the discussion relevant to Fig. 5, the local heat flux is singular at $y = 0, 1$. However, the overall heat flux through the wall is finite. Similar behavior of the heat flux integral is reported in refs. [3–6]. Increasing $A$ while keeping the values of $E$ and $B$ constant enhances heat transfer until a plateau is reached for large values of $A$. This plateau corresponds to the case where the wall temperature is identical to the temperature of the condensation reservoir ($T_w = \frac{1}{2}$). In the limit of small $A$ the wall assumes the cold reservoir temperature. Setting $T_w = -\frac{1}{2}$ and repeating the analysis in the condensation side yielded an asymptotic expression for the Nusselt number

$$Nu_1/Ra_p^{1/2} = \frac{4}{3}A\left(\frac{1+B}{4}\right)^{1/4}. \tag{39}$$

This expression for $B = 0.1$ is plotted in Fig. 6. Clearly for $A < 0.1$ equation (39) is in excellent agreement with the numerical findings. The validity of equation (39) is also justified by the fact that in the extreme $B = 0$ and for $k_1 = k$, it becomes identical to the Nusselt expression reported by Rohsenow [2, 10] for film condensation along a constant temperature wall ($Nu = 0.943Ra_f^{1/4}$).

The points denoted by triangular symbols correspond to the case $A = 1$, $E = 1$ and illustrate the effect of $B$ on the overall heat transfer through the interface. An enhancement in the overall heat transfer is observed with increasing the subcooling parameter $B$. However, this effect is minimal compared to the impact of the heat flux parameter $A$.

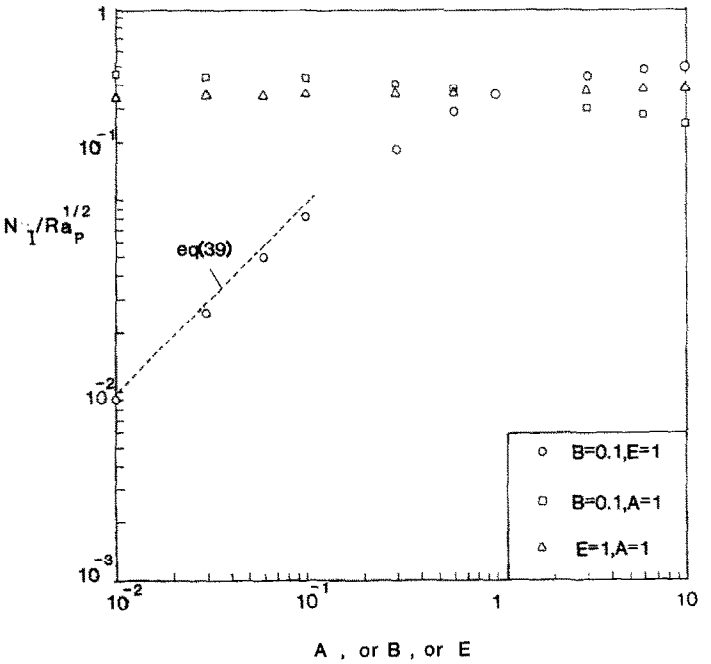


FIG. 6. Summary of heat transfer results documenting the effect of parameters $A$, $B$ and $E$ on the overall heat flux from the condensation side to the natural convection side.

The importance of parameter $E$ is also illustrated in Fig. 6 by the square symbols. Increasing $E$ causes a decrease in the value of $NuRa_p^{-1/2}$. Examining the definition of $E$, equation (5), we realize that, if $Da$ is fixed, increasing $E$ is equivalent to increasing $Ra_p$. Therefore, it is reasonable to expect a respective increase in the overall heat transfer through the wall ($Nu_I$). It can be easily proved by using the values of $Nu_I Ra^{-1/2}$ reported in Fig. 6 as well as the definition of $E$, equation (5), that such increase indeed takes place. However, the dependence of $Nu_I$ on $Ra_p$ is weaker than $Ra_p^{1/2}$, thus explaining the decrease in $Nu_I Ra^{-1/2}$ with increasing $E$.

The main results of Part II of this paper, pertaining to the geometry in Fig. 1b were qualitatively similar to the results of Part I. In particular, the effect of parameters $G$, $D$ and $N$ is analogous to the effect of parameters $A$, $B$ and $E$, respectively [21]. To avoid repetition, only the heat transfer findings for Part II will be discussed. These findings are reported in Fig. 7. The Nusselt number is defined in a manner analogous to equation (38).

$$Nu_{II} = \frac{Q_{II}}{k(T_s - T_c)} \tag{40}$$

where $k$ is fluid conductivity in the natural convection side. The rest of the quantities have been defined earlier. As shown in Fig. 7, parameters $G$ and $D$ affect the overall heat transfer much like parameters $A$ and $B$ in Part I. In the limit of large $G$ the wall takes on the temperature of the condensation reservoir ($T_w = \frac{1}{2}$). Focusing on the natural convection (open) side and repeating the analysis while keeping $T_w = \frac{1}{2}$ yields an asymptotic analytical expression for the Nusselt number [3]

$$Nu_{II} = 0.621 Ra^{1/4}. \tag{41}$$

Expression (41) agrees well with the numerical results for $G > 10$. In the limit of small $G$ the wall temperature becomes $T_w = -\frac{1}{2}$. Due to the algebraic complexity of the equations in this limit it is not possible to obtain an analytical relation for $Nu_{II}$. However, numerical results for $Nu$ for small values of $G$ ($G < 0.1$) and for $T_w = -\frac{1}{2}$ proved to be practically identical to the values of $Nu_{II}$ reported in Fig. 7. Examining the effect of parameter $N$ we see that increasing $N$ increases $Nu_{II} Ra^{-1/4}$.

## 5. FINITE THERMAL RESISTANCE AT THE INTERFACE

In this section the presence of a wall with finite thermal resistance at the porous–open interface is considered. In this case the two sides of the wall are at different temperatures, $\hat{T}_{wL}$ and $\hat{T}_{wR}$, where L and R stand for left and right, respectively. The $x$-temperature distribution in the wall bridging the gap between $\hat{T}_{wL}$ and $\hat{T}_{wR}$ is linear. In addition, the heat flux at each side is continuous. Using the heat flux continuity condition at the condensation face of the wall (for simplicity), a relation between $\hat{T}_{wL}$ and $\hat{T}_{wR}$ is obtained. This relation for the first part of the study reads

$$T_{wL} = \frac{T_{wR}\zeta + 0.5\omega_I}{\zeta + \omega_I}, \tag{42}$$

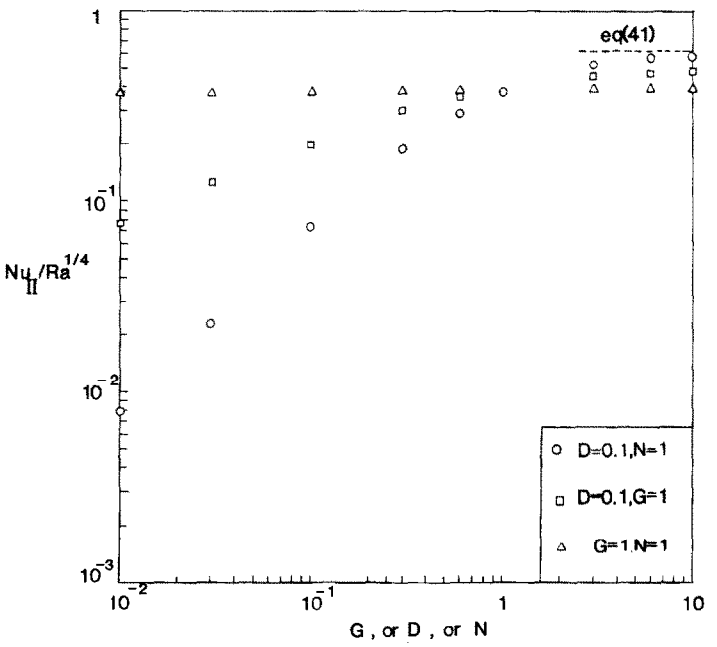


FIG. 7. Summary of heat transfer results. The effect of $G$, $D$ and $N$ on the overall heat flux across the interface.

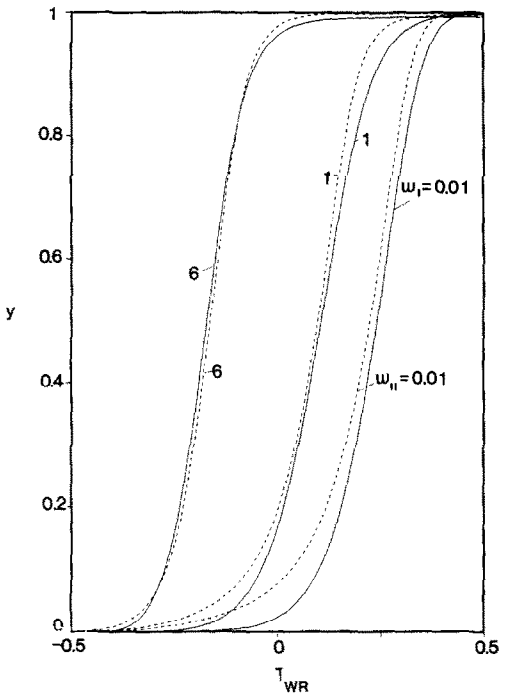


FIG. 8. The effect of the thermal resistance parameters $\omega_I$ and $\omega_{II}$ on the wall temperature distribution. The solid lines illustrate the effect of $\omega_I$ for $A = 1$, $B = 0.1$, $E = 1$ and the dashed lines the effect of $\omega_{II}$ for $G = 1$, $D = 0.1$, $N = 1$.

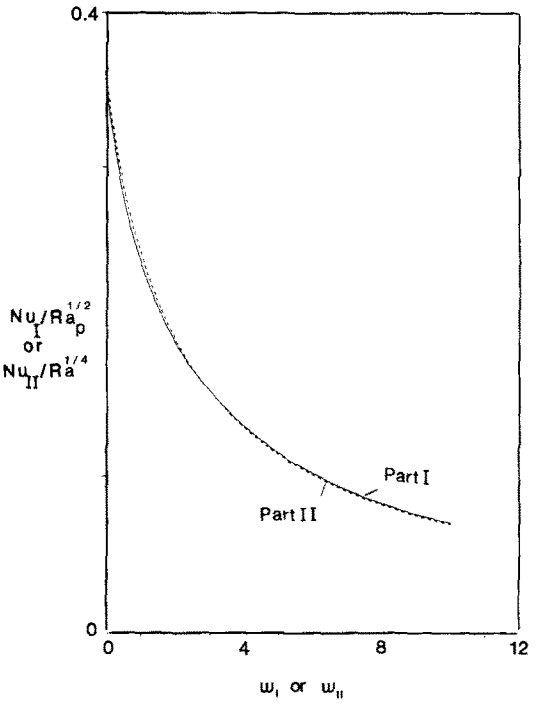


FIG. 9. The effect of $\omega_I$ (solid line for $A = 1$, $B = 0.1$, $E = 1$) and $\omega_{II}$ (dashed line for $G = 1$, $D = 0.1$, $E = 1$) on the overall heat flux through the interface.

$$\omega_I = \frac{k_I t}{HRa_f^{-1/4} k_w} \tag{43}$$

where $\omega_I$ is the wall thermal resistance parameter. In the second part of the study the corresponding relations are

$$T_{wL} = \frac{T_{wR}\bar{\zeta} + 0.5\omega_{II}}{\bar{\zeta} + \omega_{II}}, \tag{44}$$

$$\omega_{II} = \frac{k_{pI} t}{HRa_{pf}^{-1/2} k_w}. \tag{45}$$

Note that as $\omega_I, \omega_{II}$ decrease, equations (42) and (44) respectively, reflect the fact that the wall thermal resistance is negligible.

Next, the matching conditions for the heat flux at the wall need to be rederived to take into account the fact that there is a temperature gradient in the horizontal direction within the wall [21]. Finally, the wall temperature $T_w$ should be replaced by $T_{wL}$ in the equations relevant to condensation and by $T_{wR}$ in the equations relevant to natural convection. The remainder of the problem formulation remains unchanged. The numerical solution proceeds as before with $T_{wL}, T_{wR}$ connected via equation (42) for Part I and equation (44) for Part II of the problem.

The main results documenting the effect of finite thermal resistance at the interface are shown in Figs. 8 and 9. The solid lines in Figs. 8 and 9 correspond to Part I and the dashed lines to Part II of the present study. In both cases, as expected, increasing the wall thermal resistance reduces the wall temperature at all points along the vertical, relative to the zero thermal resistance limit (Fig. 8). The overall heat flux through the wall decreases with increasing the wall thermal resistance (Fig. 9). The impact of the thermal resistance on the Nusselt number in both parts of the study becomes less pronounced for $\omega_I$ or $\omega_{II}$ greater than approximately 5.

## 6. CONCLUSIONS

This paper reported a theoretical study on the phenomenon of interaction between film condensation and boundary-layer natural convection along the interface between a porous and a fluid space. Two distinct configurations were investigated. In the first configuration the natural convection phenomenon evolved in the porous space and the condensation phenomenon in the open space. The second configuration represented the opposite situation. The Brinkman-modified Darcy model was used to describe the flow in the porous medium. This model satisfies the no-slip condition on the solid wall and is believed to be appropriate for flows in the neighborhood of solid boundaries. Representative results for the wall temperature, the wall heat flux and the temperature and velocity variation across the natural convection boundary layer, and the condensation film were

reported in the course of the study. The heat transfer phenomenon across the interface is completely described by dimensionless parameters $A$, $B$ and $E$ in the first part of the study, and parameters $G$, $D$ and $N$ in the second part. Out of the above two groups of dimensionless parameters, $A$ and $G$ appear to have the strongest impact on the heat and fluid flow characteristics of the problem. Dimensionless group $A$ measures the heat transfer effectiveness of the condensation film in the open space relative to the natural convection boundary layer in the porous medium. Dimensionless group $G$, on the other hand, weighs the heat transfer effectiveness of the condensation film in the porous medium relative to the open space natural convection boundary layer. It was proved that large values of $A$ or $G$ ($A, G \to \infty$) correspond to the case of natural convection along a wall at constant temperature, that of the condensation reservoir. Similarly, small values of $A$ or $G$ ($A, G \to 0$) are relevant to film condensation from a vertical wall at constant temperature, that of the natural convection reservoir. Asymptotic analytical expressions for the overall heat transfer rate through the wall for small values of $A$ [equation (39)] and large values of $G$ [equation (41)] were also reported and found to be in agreement with the numerical calculations for $A < 0.1$ and $G > 10$.

In the last part of the paper the presence of a wall with finite thermal resistance at the interface was considered. The effect of this thermal resistance was illustrated by means of the wall thermal resistance parameter $\omega_{\mathrm{I}}$ for the first part of the study and $\omega_{\mathrm{II}}$ for the second part. As expected, increasing $\omega_{\mathrm{I}}$ or $\omega_{\mathrm{II}}$ reduces the heat leak from the warm to the cold reservoir.

*Acknowledgement*—We are grateful to NSF for providing support for this research through Grant ENG-8451144.

## REFERENCES


1. G. S. H. Lock and R. S. Ko, Coupling through a wall between two free convective systems, *Int. J. Heat Mass Transfer* **16,** 2087–2096 (1973).
2. W. M. Rohsenow, J. P. Hartnett and E. Ganic (Editors), *Heat Transfer Fundamentals*, 2nd edn. McGraw-Hill, New York (1985).
3. A. Bejan and R. Anderson, Natural convection at the interface between a vertical porous layer and an open space, *J. Heat Transfer* **105,** 124–129 (1983).
4. A. Bejan and R. Anderson, Heat transfer across a vertical impermeable partition embedded in porous medium, *Int. J. Heat Mass Transfer* **24,** 1237–1245 (1981).
5. R. Anderson and A. Bejan, Natural convection on both sides of a vertical wall separating fluids at different temperatures, *J. Heat Transfer* **102,** 630–635 (1980).
6. A. E. Gill, The boundary layer regime for convection in a rectangular cavity, *J. Fluid Mech.* **26,** 515–536 (1966).
7. E. M. Sparrow and C. Prakash, Interaction between internal natural convection in an enclosure and an external natural convection boundary layer flow, *Int. J. Heat Mass Transfer* **24,** 875–907 (1981).
8. S. Ostrach, Natural convection in cavities and cells, *Proc. Seventh Int. Heat Transfer Conference*, Keynote Paper, Munich (1982).
9. I. Catton, Natural convection in enclosures, *Proc. Sixth Int. Heat Transfer Conference*, Toronto, 1978, Vol. 6, pp. 13–49 (1979).
10. W. M. Rohsenow, Heat transfer and temperature distribution in laminar film condensation, *J. Heat Transfer* **78,** 1645–1648 (1956).
11. P. Cheng, Heat transfer in geothermal systems, *Adv. Heat Transfer* **14,** 1–105 (1979).
12. M. A. Combarnous, Natural convection in porous media and geothermal systems, *Proc. Seventh Int. Heat Transfer Conference*, Munich, Vol. 6, pp. 45–59 (1982).
13. P. Cheng and W. J. Minkowycz, Free convection about a vertical flat plate embedded in a saturated porous medium with application to heat transfer from a dike, *J. geophys. Res.* **82,** 2040–2044 (1977).
14. E. M. Sparrow and M. Faghri, Parallel flow and counterflow on an internally cooled vertical tube, *Int. J. Heat Mass Transfer* **23,** 759–762 (1980).
15. D. A. Nield, The boundary correction of the Rayleigh–Darcy problem: limitations of the Brinkman equation, *J. Fluid Mech.* **128,** 37–46 (1983).
16. C. W. Somerton and I. Catton, On the thermal instability of superposed porous and fluid layers, *J. Heat Transfer* **104,** 160–165 (1982).
17. C. T. Hsu and P. Cheng, The Brinkman model for natural convection about a semi-infinite vertical flat plate in a porous medium, *Int. J. Heat Mass Transfer* **28,** 683–697 (1985).
18. A. Bejan, *Convection Heat Transfer*. John Wiley, New York (1984).
19. D. Poulikakos and A. Bejan, Unsteady natural convection in a porous layer, *Physics Fluids* **26,** 1183–1191 (1983).
20. A. Bejan and D. Poulikakos, The non-Darcy regime for vertical boundary layer natural convection in a porous medium, *Int. J. Heat Mass Transfer* **27,** 717–722 (1984).
21. P. Sura, Interaction between film condensation and natural convection at the interface between a porous and a fluid reservoir. M.S. thesis, Mechanical Engineering Department, University of Illinois at Chicago (1985).
22. P. Cheng, Condensation along an inclined surface in a porous medium, *Int. J. Heat Mass Transfer* **14,** 983–990 (1981).
23. E. M. Parmentier, Two-phase natural convection adjacent to a vertical heated surface in a permeable medium, *Int. J. Heat Mass Transfer* **22,** 849–855 (1979).
24. T. W. Tong and E. Subramanian, A boundary layer analysis for natural convection in vertical porous enclosures—use of the Brinkman-extended Darcy model, *Int. J. Heat Mass Transfer* **28,** 563–571 (1985).
25. B. Carnahan, L. A. Luther and J. O. Wilkes, *Applied Numerical Methods*. John Wiley, New York (1969).
26. J. H. Ferziger, *Numerical Methods for Engineering Application*. John Wiley, New York (1981).


## APPENDIX

$$\frac{\mathrm{d}y}{\mathrm{d}T_{\mathrm{w}}} = \frac{a_{11}\zeta^3[1+B(\frac{1}{2}-T_{\mathrm{w}})]}{a_{14}\zeta^3[1+B(\frac{1}{2}-T_{\mathrm{w}})]-a_9(T_{\mathrm{w}}-\frac{1}{2})} \tag{A1}$$

$$\frac{\mathrm{d}\zeta}{\mathrm{d}T_{\mathrm{w}}} = \frac{a_{11}(T_{\mathrm{w}}-\frac{1}{2})}{a_{14}\zeta^3[1+B(\frac{1}{2}-T_{\mathrm{w}})]-a_9(T_{\mathrm{w}}-\frac{1}{2})} \tag{A2}$$

where

$$a_1 = 4AE$$

$$a_2 = (T_{\mathrm{w}}-0.5)/[(T_{\mathrm{w}}+0.5)\zeta]$$

$$a_3 = a_1 a_2$$

$$a_4 = (16E+a_3^2)^{1/2}$$

$$a_5 = a_3 - a_4 + 8E/a_3$$

$$a_6 = \frac{2a_3a_4-(a_3^2+a_4^2)}{a_4}$$

$$a_7 = a_4^2-a_4a_3$$

$$a_8 = \frac{a_7a_5+(a_7+8E)a_6}{a_5}$$

$$a_9 = \frac{(T_w+0.5)a_8}{\zeta}$$

$$a_{10} = \frac{a_8}{(T_w-0.5)}$$

$$a_{11} = 2a_7-a_{10}$$

$$a_{12} = [a_5a_3A(T_w-0.5)]/[(T_w+0.5)\zeta]$$

$$a_{13} = (a_{12})^2$$

$$a_{14} = \frac{a_{13}}{2E} \qquad \text{(A3)}$$

$$\frac{dy}{dT_w} = \{-\bar{\zeta}(\operatorname{sech}^2 N\bar{\zeta}-1)[2N\bar{\zeta}\cosh N\bar{\zeta}(\tanh N\bar{\zeta}-N\bar{\zeta}) + D(\tfrac{1}{2}-T_w)(1-2\cosh N\bar{\zeta}-N^2\bar{\zeta}^2\cosh N\bar{\zeta})] \times 2\bar{\zeta}^4(T_w-\tfrac{1}{2})(\tfrac{1}{2}+T_w)^4(2-T_w)\} \div \{(2G)^4(\tfrac{1}{2}-T_w)^6\bar{\zeta}(\operatorname{sech}^2 N\bar{\zeta}-1)[2N\bar{\zeta}\cosh N\bar{\zeta} \times (\tanh N\bar{\zeta}-N\bar{\zeta})+D(\tfrac{1}{2}+T_w)(1-2\cosh N\bar{\zeta} -N^2\bar{\zeta}^2\cosh N\bar{\zeta})]+3(\tfrac{1}{2}+T_w)^5(\tfrac{1}{2}-T_w)^3 \times [2N\bar{\zeta}\cosh N\bar{\zeta}(\tanh N\bar{\zeta}-N\bar{\zeta})]\} \qquad \text{(A4)}$$

$$\frac{d\bar{\zeta}}{dT_w} = \{2\bar{\zeta}^4(T_w-\tfrac{1}{2})(T_w+\tfrac{1}{2})^5(2-T_w)[2N\bar{\zeta}\cosh N\bar{\zeta} \times (\tanh N\bar{\zeta}-N\bar{\zeta})]\}/\{(2G)^4(\tfrac{1}{2}-T_w)^6\bar{\zeta} \times (\operatorname{sech}^2 N\bar{\zeta}-1)[2N\bar{\zeta}\cosh N\bar{\zeta}(\tanh N\bar{\zeta}-N\bar{\zeta}) +D(\tfrac{1}{2}-T_w)(1-2\cosh N\bar{\zeta}-N^2\bar{\zeta}^2\cosh N\bar{\zeta})] +3(\tfrac{1}{2}+T_w)^5(\tfrac{1}{2}-T_w)^3[2N\bar{\zeta}\cosh N\bar{\zeta}(\tanh N\bar{\zeta}-N\bar{\zeta})]\}. \qquad \text{(A5)}$$

## CONDENSATION EN FILM ET CONVECTION NATURELLE CONJUGEE A L'INTERFACE ENTRE MILIEU POREUX ET ESPACE OUVERT

**Résumé**—On décrit une étude théorique centrée sur l'interaction entre condensation en film et convection naturelle le long d'une paroi verticale séparant un volume de fluide d'un milieu poreux saturé de fluide. Les deux réservoirs sont maintenus à des températures différentes. L'étude est en deux parties: dans la première, le phénomène de condensation prend place dans le réservoir de fluide et la convection naturelle dans la couche poreuse. Dans la seconde partie, on considère la situation opposée. Les principales caractéristiques de couches à contre-courant, le film de condensation et la couche limite de convection naturelle sont précisées pour un large domaine des paramètres du problème. Ces paramètres apparaissent après traitement des équations. Des résultats importants pour l'ingéniérie concernant le flux global thermique entre le côté condensation et le côté convection naturelle sont résumés dans cette étude. Finalement, l'effet de la résistance thermique de la paroi, constituant la séparation des deux réservoirs, sur le flux thermique global entre les deux côtés est déterminé.

## GEKOPPELTE FILMKONDENSATION UND NATÜRLICHE KONVEKTION AN DER GRENZFLÄCHE ZWISCHEN EINEM PORÖSEN UND EINEM OFFENEN RAUM

**Zusammenfassung**—Diese Arbeit berichtet über eine theoretische Untersuchung, die sich speziell mit der Wechselwirkung von Filmkondensation und natürlicher Konvektion an einer senkrechten Wand, die ein Fluidreservoir von einem fluidgesättigten porösen Medium trennt, befaßt. Beide Reservoirs haben unterschiedliche Temperaturen. Die Untersuchung besteht aus zwei Teilen: Im ersten Teil findet der Kondensationsvorgang im Fluidreservoir statt, die natürliche Konvektion in der porösen Schicht. Im zweiten Teil wird die umgekehrte Situation betrachtet. Die wichtigsten Wärmeübertragungs- und Strömungscharakteristiken in den beiden Gegenstromschichten, dem Kondensatfilm und der Grenzschicht der natürlichen Konvektion, werden über einen weiten Parameterbereich dokumentiert. Diese Parameter werden durch Grenzschichtformulierung der Bilanzgleichungen erhalten. Wichtige ingenieurmäßige Ergebnisse bezüglich des Gesamtwärmestroms von der Kondensationsseite zur Seite der natürlichen Konvektion werden in der Untersuchung betrachtet. Schließlich wird der Einfluß des thermischen Widerstandes der Wand, die die Grenzfläche zwischen den beiden Reservoirs bildet, auf den Gesamtwärmestrom zwischen der Kondensationsseite und der Seite der natürlichen Konvektion berechnet.

## СОПРЯЖЕННАЯ ПОСТАНОВКА ЗАДАЧИ О ПЛЕНОЧНОЙ КОНДЕНСАЦИИ И ЕСТЕСТВЕННОЙ КОНВЕКЦИИ ВДОЛЬ ГРАНИЦЫ МЕЖДУ ПОРИСТЫМ СЛОЕМ И ОТКРЫТЫМ ПРОСТРАНСТВОМ

**Аннотация**—Теоретически исследовано взаимодействие между пленочной конденсацией и естественной конвекцией вдоль вертикальной стенки, отделяющей резервуар, заполненный жидкостью, от пористого резервуара, насыщенного жидкостью. Оба резервуара поддерживаются при разных температурах. Работа состоит из двух частей: в первой исследуются конденсация в резервуаре с жидкостью и естественная конвекция в пористом слое, во второй части рассматривается обратная ситуация. Основные характеристики теплопереноса и течения в двух противоточных слоях, т.е. пленке конденсата и пограничном слое со свободной конвекцией, определены для широкого диапазона параметров задачи. Эти параметры появляются после представления определяющих уравнений в приближении пограничного слоя. Обобщены результаты, касающиеся суммарного теплового потока от резервуара, где происходит конденсация, к слою с естественной конвекцией. Определено влияние теплового сопротивления стенки, составляющей поверхность раздела между двумя резервуарами, на общий тепловой поток.